Over 17.1% or 18.2% efficiency of layer-by-layer all-polymer solar cells via incorporating efficient Pt complexes as energy donor additive

Lu Zhang,[a] Miao Zhang,[b]* Yuheng Ni,[a] Wenjing Xu,[a] Hang Zhou,[a] Shengyi Ke,[b] Hongyue Tian,[a] Sang Young Jeong,[c] Han Young Woo,[c]* Wai-Yeung Wong,[b]* Xiaoling Ma,[a,d]* and Fujun Zhang[a,d]*

[a] Key Laboratory of Luminescence and Optical Information, Ministry of Education, Beijing Jiaotong University, 100044, Beijing, China. E-mail: maxl@bjtu.edu.cn; fjzhang@bjtu.edu.cn

[b] Department of Applied Biology and Chemical Technology, The Hong Kong Polytechnic University, Hung Hom, Hong Kong 999077, People's Republic of China. E-mail: bjtumiao.zhang@polyu.edu.hk; wai-yeung.wong@polyu.edu.hk

[c] Organic Optoelectronic Materials Laboratory, Department of Chemistry, College of Science, Korea University, Seoul, 02841, Republic of Korea. E-mail: hywoo@korea.ac.kr

[d] Tangshan Research Institute of Beijing Jiaotong University, Tangshan, 063000, People's Republic of China.

Abstract:

In this work, layer-by-layer (LbL) all-polymer solar cells (APSCs) are constructed with or without the incorporation of a Pt complex F-Pt as an energy donor additive in the acceptor layer. The power conversion efficiency (PCE) of LbL APSCs can be enhanced from 15.86% to 17.14% through introducing 0.2 wt% F-Pt in PY-IT layer, originating from the efficient energy transfer from F-Pt to PM6 and PY-IT. The efficient energy transfer from F-Pt to PM6 and PY-IT can be well confirmed from the spectral overlapping between photoluminescence (PL) spectra of F-Pt and absorption spectra of PM6 and PY-IT, as well as the prolonged PL lifetime of PM6 and PY-IT according to the transient time resolved PL spectra of blend and LbL films. The prolonged lifetime of PM6 and PY-IT should be conducive to increase exciton diffuse length and exciton dissociation in the LbL APSCs doped F-Pt. The universality of F-Pt incorporation strategy can be further confirmed from PBQx-TCl/PY-DT based LbL APSCs, the PCE can be increased from 17.57% to 18.29% by incorporating F-Pt into PY-DT layer.

Introduction

Organic solar cells (OSCs) are considered as a suitable candidates for next generation energy-harvesting devices due to their advantages of abundance of raw materials, low cost, mechanical flexibility and ease of solution processing.[1-5] The micro/nano-scale phase separation of active layers plays an important role in photogenerated exciton dissociation and charge transport in the bulk

heterojunction (BHJ) OSCs. In fact, there is great challenge to well optimize the molecular arrangement and phases separation degree of donors and acceptors by employing blend solutions with the same film-drying process. Layer-by-layer (LbL) active layers were prepared by sequential spin-coating technology, which endows the active layer with favorable vertical composition distribution, tunable D/A interfaces and high phase purity in donor or acceptor layer.[6-11] The efficient exciton dissociation in LbL all-polymer solar cells (APSCs) is a challenge due to the quite limited exciton diffusion distance in organic materials and the relatively small donor/acceptor interface in LbL devices.[12-15] Some smart strategies of enhancing LbL exciton dissociation focus on increasing the interface of donor layer and acceptor layer, such as enlarging component interdiffusion between donor and acceptor layers by solvent additive, introducing dissociation strengthening layer (DSL) or employing donor incorporation into acceptor layer (DIA) strategy.[16-22] It is well known that exciton diffusion distance strongly depends on the exciton lifetime of donors and acceptors, which should be prolonged by increased the exciton lifetime of donors and acceptors through incorporating efficient triplet materials with long emission lifetime. Liao group reported that delayed fluorescence (DF) material was incorporated to BHJ active layers for improving the lifetime of excitons, leading to the PCE improvement.[23] The energy transfer from donor to acceptor also provides an additional path to improve the exciton dissociation efficiency, which was been reported in the previous works.[24-27] Triplet materials always have strong PL emission in the visible and near infrared light range, and efficient energy transfer from triplet materials to donors or acceptors will be conducive to increase the performance of LbL PSCs. Here, typical works on OPVs with triplet material as donor, acceptor or additive are summarized in **Table 1**. In 2019, Peng et al. proposed a new strategy of platinum(II) complexation and got a PCE of 16.35% by Pt-containing donor Pt10 and micromolecular acceptor Y6.[28] In this work, 17.1% or 18.2% efficiency can be achieved from PM6/PY-IT or PBQx-TCl/PY-DT based LbL PSCs via incorporating 8',10'-difluoro-4,6-dimethyl-6'λ4,3λ3,5'λ4-spiro[1,3,4,5,6,2-dioxatriplatinine-2,6'-benzo[c]pyrimido[1,2-][1,2,3,4,5] azatriplati-nole] (F-Pt).

Table 1. Typical works on BHJ OPVs with triplet material

Structure	Materials	J_{SC} [mA·cm^{-2}]	V_{OC} [V]	FF [%]	PCE [%]	Ref.
BHJ	P3HT:ICBA	10.44	0.859	68.5	6.15	29
	P3HT:ICBA:**Ir(ppz)$_3$**	12.4	0.855	66.7	7.08	
	PBDB-T:PCBM	10.68	0.86	72.3	6.67	30

	PBDB-T:**BFPTP**	12.83	0.94	62.4	7.52	
	PTB7-Th:$PC_{71}BM$	14.98	0.81	65.1	7.92	31
	PTB7-ThPt1.5:$PC_{71}BM$	16.21	0.8	65.01	8.45	
	P1-PTB7Ir0:$PC_{71}BM$	16.71	0.71	56	6.64	32
	P1-PTB7Ir1:$PC_{71}BM$	18.14	0.75	64	8.71	
	PTB7:$PC_{71}BM$	13.3	0.75	71.7	7.37	33
	PTB7:**Ir-Orange**:$PC_{71}BM$	16.1	0.74	72.9	8.72	
	PTB7-Th:$PC_{71}BM$	14.98	0.81	65.1	7.92	34
	PTB7-ThIr1:$PC_{71}BM$	16.6	0.8	69.36	9.19	
	eBz3Ir:L8-BO	15.51	0.83	50.39	6.46	35
	eTBz3Ir:L8-BO	21.64	0.83	58.26	10.48	
	Pt0:Y6	25.1	0.8	64.9	13.03	28
	Pt10:Y6	26.45	0.81	76.3	16.35	
	PM6:Y6	25.21	0.84	73.71	15.65	36
	PM6Ir1:Y6	26.16	0.85	75.33	16.71	
	PM6Ir1:N3	26.13	0.84	74.11	16.27	37
	PM6Ir1:N3:ITIC-Th	26.53	0.86	75.47	17.22	
LbL	PM6/PY-IT	22.95	0.95	72.75	15.86	This work
	PM6/PY-IT:**F-Pt**	24.42	0.95	73.87	17.14	
	PBQx-TCl/PY-DT	24.53	0.96	74.68	17.57	
	PBQx-TCl/PY-DT:**F-Pt**	24.79	0.96	76.53	18.29	

In this work, series of LbL APSCs were fabricated with a device structure of ITO/ Poly(3,4-ethylenedioxythiophene): poly (styrene sulfonate) (PEDOT:PSS)/ active layer/ Poly[(9,9-bis(3'-(N,Ndimethylamino)propyl)-2,7-fluorene)-alt-5,5-bis(2,2'-thiophene)-2,6-naphthalene-1,4,5,8-tetracaboxylic-N,N'-di(2-ethylhexyl)imide] (PNDIT-F3N)/ Ag, where the active layer is composed of Poly[(2,6-(4,8-bis(5-(2-ethylhexyl-3-fluoro)thiophen-2-yl)-benzo[1,2-b:4,5-b']dithiophene))-alt-(5,5-(1',3'-di-2-thienyl-5',7'-bis(2-ethylhexyl)benzo[1',2'-c:4',5'-c']dithiophene-4,8-dione)] (PM6) layer and sequentially deposited Poly[2,2'-((2Z,2'Z)-((12,13-bis(2-octyldodecyl)-3,9-diundecyl-12,13dihydro[1,2,5]thiadiazolo[3,4e]thieno[2",3":4',5']thieno[2',3':4,5]pyrrolo[3,2-g]thieno[2',3':4,5]thieno[3,2-b]-indole-2,10-diyl)bis(methanylylidene))bis(5-methyl-3-oxo-2,3-dihydro-1H-indene-2,1-diylidene)) dimalononitrile-co-2,5-thiophene] (PY-IT) layer with and without F-Pt. The chemical structures and energy levels of PM6, PY-IT and F-Pt are displayed in **Figure 1a** and **Figure 1b**, respectively.[38] The normalized absorption spectra of neat PM6, PY-IT and F-Pt films, as well as the normalized PL spectrum of F-Pt film are shown in **Figure 1c**. It is apparent that neat F-Pt film has strong photon harvesting capability in the wavelength from 300 to 500 nm and exhibits strong photoluminescence (PL) emission covering from 550 to 750 nm. There is large spectral overlapping between F-Pt PL spectrum and absorption spectra of PM6 and PY-IT, which should be favored to the fluorescence resonance energy transfer (FRET) from F-Pt to PM6 or PY-IT.[39] It is well known that the intermolecular distance also influences the FRET efficiency,

intermolecular compatibility of used materials was characterized by contact angle experiment. The contact angles of PM6, PM6:F-Pt, PY-IT, PY-IT:F-Pt and F-Pt films are shown in **Figure 1d** and the surface energy and interfacial energy calculated by contact angles are summarized in **Table S1**. The surface energy values of neat PM6, PY-IT and F-Pt films are calculated to be 29.4, 34.4, and 37.9 mN·m^{-1}, respectively. The interfacial energy ($\gamma_{X:Y}$) between PM6 and F-Pt is 2.64 mN·m^{-1} and $\gamma_{PY\text{-}IT:F\text{-}Pt}$ is 1.41 mN·m^{-1}, which indicates that F-Pt has better compatibility with PY-IT. The similar $\gamma_{PM6:PY\text{-}IT}$ of 0.48 mN·m^{-1} and $\gamma_{PM6:PY\text{-}IT+F\text{-}Pt}$ of 0.49 mN·m^{-1} indicates that the wettability between PM6 layer and PY-IT layer F-Pt is hardly influenced by incorporating small content F-Pt in PY-DT layer. To further confirm the positive effect of F-Pt on performance improvement of LbL all-PSC, the champion PCE of 18.29% is achieved from PBQx-TCl/PY-DT:F-Pt as the LbL active layers. Over 8% or 4% PCE improvement can be obtained by incorporating appropriate F-Pt as energy donor additive in PM6 or PBQx-TCl based LbL APSCs. This work provides a novel strategy to improve the performance of LbL APSCs by incorporating appropriate triplet material as energy donor additive to improve photon utilization efficiency.

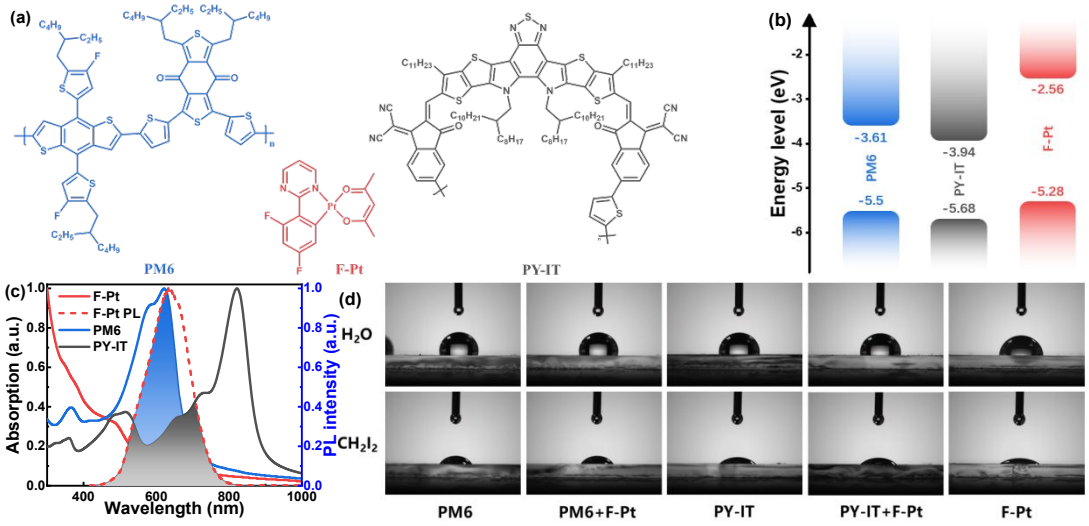

Figure 1. a, b) Chemical structures and energy levels of PM6, PY-IT, and F-Pt. **c)** Absorption spectra of PM6, PY-IT, F-Pt films and normalized PL spectrum of F-Pt. **d)** Images of contact angles of neat and blend films.

Results and discussion

The current density-voltage (*J*-*V*) curves of LbL APSCs with or without F-Pt were measured under simulated AM 1.5 G illumination, as depicted in **Figure 2a**. The detailed parameters of LbL APSCs are summarized in **Table 2**. It is apparent that open circuit voltage (V_{OC}) of LbL APSCs can

be kept constant with or without F-Pt incorporation in PY-IT layer. The PCE of the control LbL APSCs without F-Pt is 15.86% with a J_{SC} of 22.95 mA/cm^2 and FF of 72.75%, which is close to the reported values of the same materials based LbL APSCs.[17] The J_{SC} and FF of LbL APSCs can be slightly increased and then decreased along with more F-Pt incorporated content in PY-IT layers. A champion PCE of 17.17% is achieved from the LbL APSCs with 0.2 wt% F-Pt content in PY-IT layer, contributing from the optimized J_{SC} of 24.42 mA·cm^{-2} and FF of 73.87%. To better understand the FF variation dependence on F-Pt content in PY-IT layer, shunt resistance (R_{SH}) and series resistance (R_S) of APSCs are calculated according to the corresponding *J-V* curves and are listed in **Table 2**. The optimized LbL APSCs show the lowest R_S of 2.58 Ω·cm^2 and the highest R_{SH} of 1135 Ω·cm^2, which is conducive to charge transport in the LbL active layers for achieving a relatively high FF. The PCE of the LbL APSCs with 0.2 wt% F-Pt in donor layer is 14.42% with a J_{SC} of 21.49 mA/cm^2 and FF of 70.64%. The decreased J_{SC} and FF of LbL APSCs with F-Pt in PM6 layer is caused by the poor hole transport in donor layer with large isolated hole traps, which could be proofed by the energy level of F-Pt and PM6. External quantum efficiency (EQE) spectra of LbL APSCs were measured and are depicted in **Figure 2b**. The calculated J_{SC}s are obtained by integrating the corresponding EQE spectra, which are slightly lower than the measured J_{SC} due to the attenuation of the unpackaged cells for EQE measurement in the air conditions. It should be highlighted that the EQE of LbL APSCs with F-Pt incorporation are increased in the wavelength range from 350 nm to 850 nm, which can be confirmed from the EQE spectral difference (ΔEQE) between the optimized LbL APSCs with F-Pt incorporation and the control LbL APSCs, as displayed in **Figure 2b**.

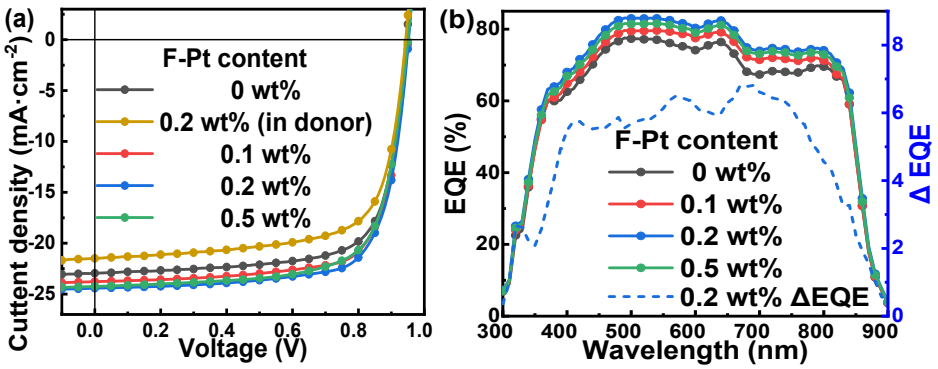

Figure 2. a) *J–V* curves and **b)** EQE spectra of PM6/PY-IT based LbL APSCs with or without F-Pt incorporation and ΔEQE between the control cells and the optimized cells.

Table 2. Parameters of PM6/PY-IT based LbL devices.

F-Pt content [wt%]	J_{SC} [mA·cm^{-2}]	Cal. J_{SC} [mA·cm^{-2}]	V_{OC} [V]	FF [%]	PCE (Ave. ±Dev.) [%]	R_S [Ω·cm^2]	R_{SH} [Ω·cm^2]
0	22.95	21.82	0.95	72.75	15.86 (15.74±0.10)	2.85	906
0.1	23.78	22.60	0.95	73.78	16.66 (16.55±0.09)	2.69	1078
0.2	24.42	23.74	0.95	73.87	17.14 (16.96±0.15)	2.58	1135
0.5	24.24	23.17	0.95	71.83	16.54 (16.34±0.17)	3.15	1024
0.2[a]	21.49	--	0.95	70.64	14.42 (14.28±0.14)	3.42	853

a) 0.2 wt% F-Pt was incorporated in donor layer.

To clarify the underlying reason of increased EQE values, PL spectra of neat PM6 and PY-IT films, blend PM6:F-Pt and PY-IT:F-Pt films were measured under 375 nm light excitation, as shown in **Figure 3a**. The PL emission intensity of PM6 and PY-IT can be increased in the blend films with 0.5 wt% F-Pt incorporation, resulting from the energy transfer from F-Pt to PM6 or PY-IT. The increased PL emission intensity of PM6 and PY-IT indicates that more excitons will be photogenerated in PM6 and PY-IT in the blend films, which should be conducive to generate more charge carrier after exciton dissociation. To further confirm the energy transfer from F-Pt to PY-IT, the time resolved PL spectra (TRPL) of neat F-Pt and PY-IT:F-Pt films were measured under 375 nm light excitation and probing the 630 nm emission from PY-IT, as exhibited in **Figure 3b**. The lifetime of PL emission of F-Pt can be markedly decreased from 33.9 ns to 1.12 ns by incorporating F-Pt into PY-IT, indicating that PL emission of F-Pt can be quenched through energy transfer from F-Pt to PY-IT. The TRPL spectra of neat PM6 film, blend PM6:F-Pt film, LbL PM6/PY-IT and PM6/PY-IT:F-Pt films were measured under 500 nm light excitation and probing 690 nm emission from PM6, as exhibited in **Figure 3c**. The PL emission lifetime of PM6 is increased from 65 ps to 134 ps for the PM6/PY-IT layer by incorporating F-Pt into PY-IT layer. Meanwhile, the PL emission lifetime of PM6 is increased from 220 ps to 265 ps by incorporating F-Pt into PM6 layer. The prolonged PL emission lifetime of PM6 should be attributed to the energy transfer from F-Pt to PM6. The similar phenomenon is also observed from the TRPL spectra of PY-IT and PM6/PY-IT films by probing 830 nm emission of PY-IT under 700 nm light excitation, as displayed in **Figure 3d**. The PL emission lifetime of PY-IT is increased from 644 ps to 1034 ps by incorporating 0.2 wt% F-Pt into PY-IT layer. Meanwhile, the PL emission lifetime of PY-IT is increased from 381 ps to 484 ps for the PM6/PY-IT films by incorporating F-Pt into PY-IT layer. It is well known that the increased lifetime of excitons on PM6 and PY-IT should be conducive to enhance exciton diffuse distance, more excitons will be dissociated into charge carriers at the interface between PM6 and

PY-IT.[40, 41]

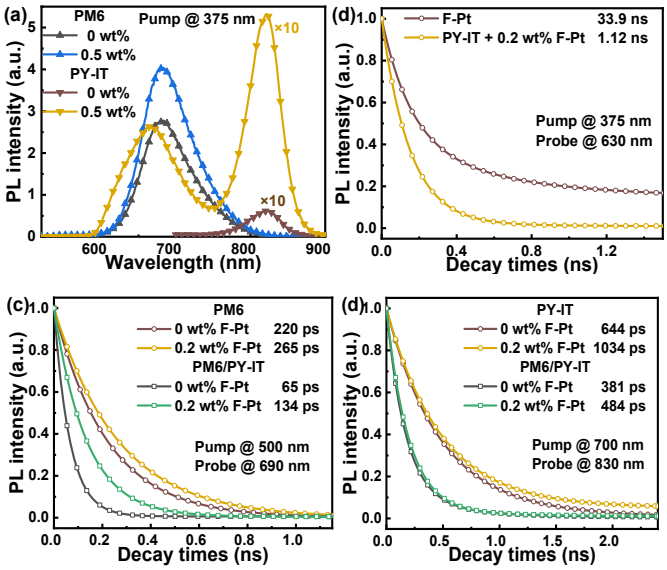

Figure 3. a) The PL spectra of PM6 and PY-IT films with or without F-Pt under 375 nm light excitation. **b)** TRPL spectra of neat F-Pt and PY-IT:F-Pt films. **c)** TRPL spectra of PM6, PM6:F-Pt, PM6/PY-IT and PM6/PY-IT:F-Pt films. **d)** The TRPL spectra of PY-IT, PY-IT:F-Pt, PM6/PY-IT and PM6/PY-IT:F-Pt films.

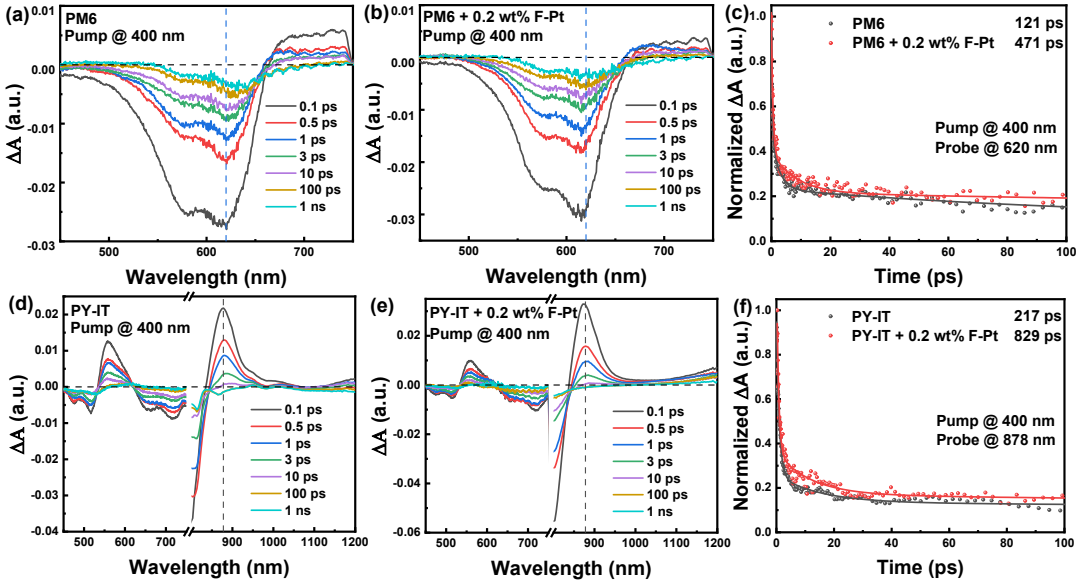

Figure 4. The TA spectra of **a)** neat PM6, **b)** PM6:F-Pt, **c)** neat PY-IT, and **d)** PY-IT:F-Pt. The decay curve of **e)** PM6 and PM6:F-Pt films at 620 nm, **f)** PY-IT and PY-IT:F-Pt films at 878 nm.

To further confirm the energy transfer from F-Pt to PM6 and PY-IT, the transient absorption (TA) spectra of PM6, PM6:F-Pt, PY-IT as well as PY-IT:F-Pt films were measured under 400 nm light excitation and shown in **Figure 4**. TA spectra consist of two main features: negative signature originating from ground state bleach (GSB) and stimulated emission (SE), and positive signature

originating from excited state absorption (ESA).[42] The TA spectra of neat PM6 and PM6:F-Pt films show an obvious GSB peak at about 620 nm, which can reflect the excited state decay dynamics of PM6. The decay dynamics of the GSB peak at 620 nm is fitted and shown in **Figure 4c**. The decay time constant of GSB peak of PM6 is increased from 121 ps to 471 ps, which should be caused by energy transfer from F-Pt to PM6. A similar phenomenon can be observed in the TA spectra of PY-IT and PY-IT:F-Pt films. The ESA peak of PY-IT at 878 nm is fitted, as exhibited in **Figure 4f**. The decay time constant of ESA peak of PY-IT is increased from 217 ps to 819 ps by incorporating 0.2 wt% F-Pt. The energy transfer from F-Pt to PM6 and PY-IT can be further confirmed from the decreased decay time constant of GSB peak of PM6 and increased decay time constant of ESA peak of PY-IT by incorporating F-Pt.

increased exciton diffuse distance by incorporating F-Pt in PY-IT layers, *J-V* curves of APSCs with the same thickness of PM6 layer were measured by producing PY-IT or PY-IT:F-Pt with graded spin-coating speed, as exhibited in **Figure S1**. The normalized PCEs and FFs of APSCs with different thick acceptor layers are displayed in **Figure 5**. It is apparent that the PCEs and FFs of APSCs with F-Pt incorporating are larger than those of APSCs without F-Pt, which should be due to the prolonged exciton diffuse distance by incorporating F-Pt in PY-IT layers. Meanwhile, APSCs with F-Pt incorporation show a relatively slow decreasing trend of PCE and FF with acceptor layer thickness increasing.

To confirm the increased exciton diffuse distance by incorporating F-Pt in PY-IT layers, *J-V* curves of APSCs with the same thickness of PM6 layer were measured by producing PY-IT or PY-IT:F-Pt with graded spin-coating speed, as exhibited in **Figure S1**. The normalized PCEs and FFs of APSCs with different thick acceptor layers are displayed in **Figure 5**. It is apparent that the PCEs and FFs of APSCs with F-Pt incorporating are larger than those of APSCs without F-Pt, which should be due to the prolonged exciton diffuse distance by incorporating F-Pt in PY-IT layers. Meanwhile, APSCs with F-Pt incorporation show a relatively slow decreasing trend of PCE and FF with acceptor layer thickness increasing.

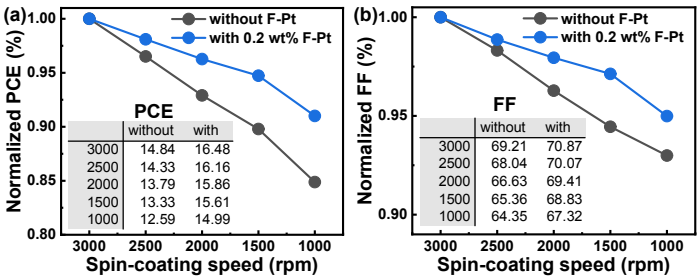

Figure 5. LbL all-PSCs with the same thickness of PM6 and different thick PY-IT layers: **a)** normalized PCEs and **b)** normalized FFs dependence on spin-coating speed of PY-IT layers.

The photocurrent density (J_{ph}) as a function of the effective voltage (V_{eff}) curves were investigated and are displayed in **Figure 6a**. The J_{ph} is defined as: $J_{ph} = J_L - J_D$, where J_L is current density under AM 1.5G simulated solar with 100 mW·cm^{-2} light intensity and J_D is current density in dark conditions. The V_{eff} is defined as: $V_{eff} = V_{0C} - V_{app}$, where V_{app} is the bias voltage. J_{ph} has three key nodes called saturation photocurrent density (J_{sat}), short-circuit photocurrent density (J_{ph}^{*}) and maximum output current density ($J_{ph}^{\&}$). The exciton dissociation efficiency (η_D) and the charge collection efficiency (η_C) can be evaluated according to the equations: $\eta_D = J_{ph}^{*}/J_{sat}$ and $\eta_C = J_{ph}^{\&}/J_{sat}$, respectively.[43-45] As listed in **Table S2**, for the LbL APSCs with 0.2 wt% F-Pt incorporation, the η_D value is increased from 94.49% to 95.11% and the η_C value is increased from 83.48% to 85.05%, indicating that the exciton dissociation and charge extraction efficiency of all-PSC can be slightly increased by incorporating appropriate F-Pt in PY-IT layers.

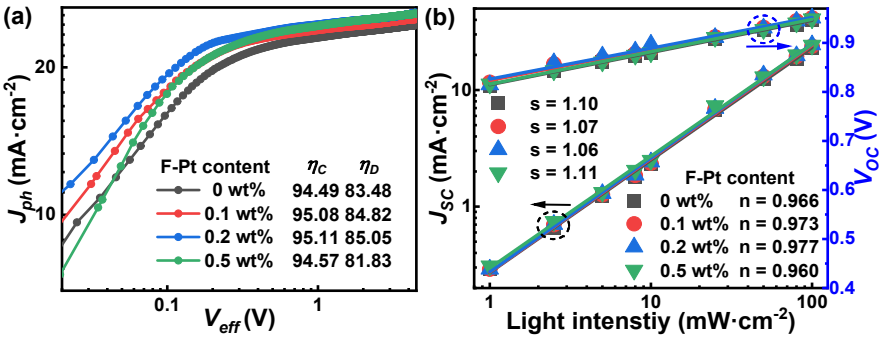

Figure 6. a) J_{ph}–V_{eff} curves of PM6/PY-IT based LbL devices. **b)** J_{SC}–P_{light} and V_{OC}–P_{light} curves of PM6/PY-IT based LbL devices.

The *J*-*V* curves of APSCs were measured under different light intensity to investigate the effect of F-Pt on the recombination dynamic process in the LbL active layers, as displayed in **Figure S2**. The J_{SC}- P_{light} and V_{OC}-P_{light} curves of LbL APSCs are displayed in **Figure 6b**. The bimolecular recombination in the active layer can be evaluated by the dependence of J_{SC} values on P_{light} expressed as:

$$J_{SC} \propto P_{light}^{n}$$

The fitting parameter (n) reflects the bimolecular recombination degree in the LbL active layers, the bimolecular recombination can be efficiently suppressed when n is close to 1.[12, 46, 47] The n value arrives to 0.977 when the F-Pt incorporating ratio is 0.2 wt% in PY-IT layer, indicated the bimolecular recombination can be efficiently suppressed by incorporating appropriate F-Pt. The dependence of V_{OC} values on P_{light} can be expressed as:

$$V_{OC} \propto s(KT/q)\ln(P_{light})$$

where K, T and q represent the Boltzmann constant, absolute temperature and elementary charge, respectively.[48] The fitting parameter (s) reflects the Shockley-Read-Hall recombination degree in the LbL active layers. When s value approaches 1, indicating the decreased Shockley-Read-Hall recombination degree.[49] It is apparent that bimolecular recombination and Shockley-Read-Hall recombination can be simultaneously decreased by incorporating 0.2 wt% F-Pt in PY-IT layer, resulting in the relatively large FF of 73.87%.

The electrochemical impedance spectroscopy (EIS) measurements were carried out to gain more insight on charge dynamic process in LbL APSCs. The Nyquist plots of LbL APSCs are displayed in **Figure 7a** and the fitting parameters are listed in **Table S3**. R_{CT} is associated with charge transfer resistance, R_{OS} represents parasitic series resistance.[50-52] The nonideal behaviors of capacitor is described by constant phase element (CPE), and the value CPE_P reflect the degree of interface defect.[53-55] The time constant (τ) is related to charge transfer, which can be expressed by: $\tau = R_{CT} \times CPE_T$.[17, 50] The APSCs incorporating 0.2 wt% F-Pt exhibits the lowest R_{CT} of 34.5 Ω and R_{OS} of 29.6 Ω, indicating the most efficient charge transport in LbL PM6/PY-IT:F-Pt layers. The CPE_P values of APSCs increased from 0.965 to 0.978 with F-Pt content in PY-IT layer up to 0.2 wt%, and then decreased to 0.948 with more F-Pt. The closest to 1 of CPE_P for the optimal APSCs suggests fewer defects at the interface due to the appropriate F-Pt incorporation in PY-IT layer. The APSCs with 0.2 wt% F-Pt shows the lowest τ value of 258 ns, which signifies inhibited charge recombination in the active layer. The transient photovoltage (TPV) curves of APSCs were measured under open-circuit conditions to further explore charge recombination degree in the active layer, as displayed in **Figure 7b**. The τ_{pho} value of LbL devices is raised from 14.86 μs to 27.81 μs by doping 0.2 wt% of F-Pt, which means a lower carrier recombination caused by F-Pt incorporating.

[56-58] Transient photocurrent (TPC) decay curves of APSCs were measured under short-circuit conditions, as displayed in **Figure 7c**. τ_{ext} shown in the figure is charge extraction time constant, which is fitted by TPC curve.[59-63] The lowest τ_{ext} of 0.23 μs in the LbL all-PSC with 0.2 wt% F-Pt means the most efficient charge collection, as confirmed from the relatively high FF of 78.87%. The experimental results of TPV, TPC and EIS show that the decreased recombination degree and more efficient charge collection can be simultaneously achieved from all-PSC with 0.2 wt% F-Pt incorporation, leading to the J_{SC}, FF and PCE improvement.

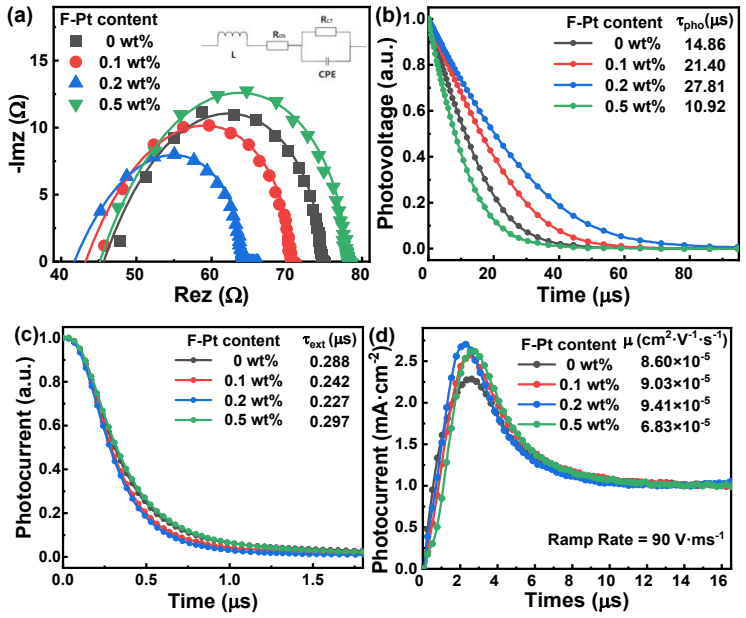

Figure 7. LbL APSCs with or without F-Pt incorporation in PY-IT layer: **a)** Nyquist plots and the equivalent circuit, the line is fitted curves; **b)** Transient photovoltage curves; **c)** transient photocurrent curves; **d)** Photo-CELIV curves.

The photo-induced charge carrier extraction in linearly increasing voltage (photo-CELIV) curves of APSCs were measured to further explain the promotion of charge extraction, as shown in **Figure 7d**. The calculated μ is increased from 8.60×10^{-5} $cm^2\cdot V^{-1}\cdot s^{-1}$ to 9.41×10^{-5} $cm^2\cdot V^{-1}\cdot s^{-1}$ and then decreased to 6.83×10^{-5} $cm^2\cdot V^{-1}\cdot s^{-1}$ with the increasing of F-Pt content from 0 wt% to 0.5 wt%, which is consistent with the previous analysis on charge collection efficiency dependence on F-Pt content. The charge mobility of PM6/PY-IT:F-Pt and PY-IT:F-Pt films were measured by using space charge limit current (SCLC) method based on the single carrier-only device structures of ITO/ZnO/Donor/Acceptor/PNDIT-F3N/Ag, ITO/PEDOT:PSS/Donor/Acceptor/MoO_3/Ag or ITO/ZnO/Acceptor/Ag.[64-67] The $\ln(Jd^3/V^2)$-$(V/d)^{0.5}$ curves of LBL devices and single acceptor layers based devices are displayed in **Figure S3**, respectively. The calculated election mobility (μ_e)

and hole mobility (μ_h) in the corresponding active layers are listed in **Table S4**. The μ_e in the LbL active layers can be slightly increased from 4.06×10^{-4} $cm^2\cdot V^{-1}\cdot S^{-1}$ to 7.33×10^{-4} $cm^2\cdot V^{-1}\cdot S^{-1}$ along with more F-Pt incorporation in PY-IT layer, the μ_h in the LbL active layers is slightly decreased from 6.37×10^{-4} $cm^2\cdot V^{-1}\cdot S^{-1}$ to 4.26×10^{-4} $cm^2\cdot V^{-1}\cdot S^{-1}$ along with more F-Pt incorporation in PY-IT layer. The increased μ_e in the LbL active layers can be further confirmed from the μ_e variation in PY-IT from 4.42×10^{-5} $cm^2\cdot V^{-1}\cdot S^{-1}$ to 6.07×10^{-5} $cm^2\cdot V^{-1}\cdot S^{-1}$ with the incorporating of F-Pt. The ratio of μ_h/μ_e of LbL active layers with PY-IT doped with 0.2 wt% F-Pt is closer to 1, indicating the more balanced charge transport in the LbL active layer. The more balanced charge transport well explains the relatively large FF of LbL APSCs with 0.2 wt% F-Pt in PY-IT layer.

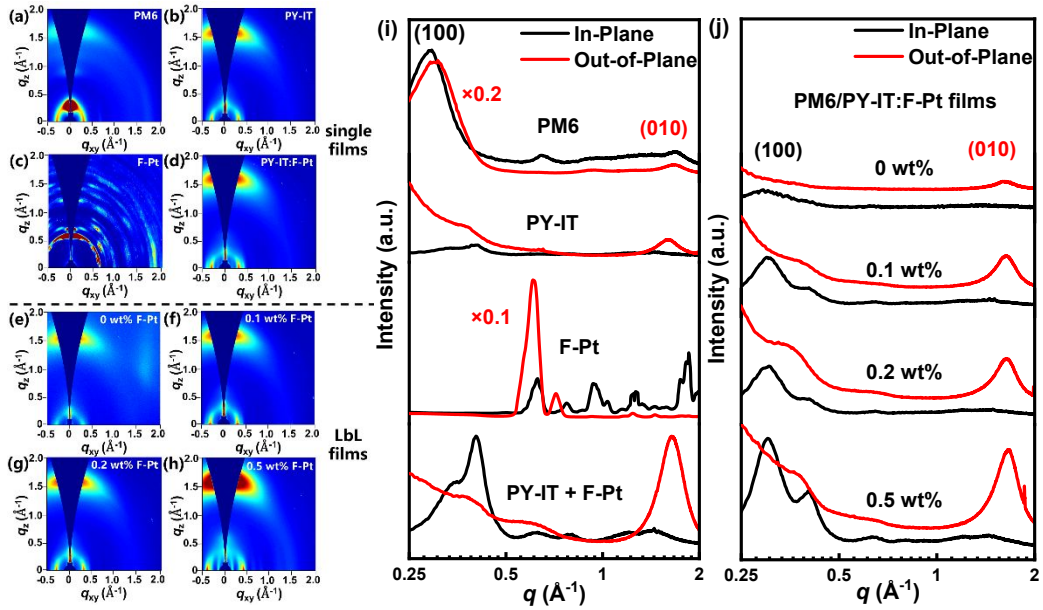

Figure 8. The 2D-GIWAXS patterns of **a)** PM6, **b)** PY-IT, **c)** F-Pt, **d)** PY-IT:F-Pt single films and **e-h)** PM6/PY-IT LbL films with or without F-Pt in acceptor layer. **i-j)** The in-plane (IP, black line) and out-of-plane (OOP, red line) profiles abstracted from 2D-GIWAXS patterns corresponding single films and LbL films.

Table 3. The diffraction vector (q) values of diffraction peaks and crystal coherence length (CCL) values in LbL films.

F-Pt content [wt%]	π-π				(100)			
	q [Å^{-1}]	d-spacing [Å]	FWHM [Å^{-1}]	CCL [Å]	q [Å^{-1}]	d-spacing [Å]	FWHM [Å^{-1}]	CCL [Å]
0	1.623	3.872	0.314	18.02	0.286	21.97	0.0927	61.03
0.1	1.625	3.866	0.308	18.34	0.299	21.01	0.0799	70.75
0.2	1.626	3.865	0.284	19.89	0.301	20.88	0.0796	71.03
0.5	1.643	3.442	0.323	17.52	0.302	20.79	0.0739	76.49

Grazing incidence wide-angle scattering (GIWAXS) characterization was carried out to investigate the effect of F-Pt incorporation on the crystallinity and molecular orientation in films. The 2D-GIWAXS images and 1D diffraction profiles along in-plane (IP) and out-of-plane (OOP) directions of neat and LbL films are displayed in **Figure 8.** The crystal coherence length (CCL) and d-spacing of π-π stacking of neat films and LbL films are shown in **Table S5** and **Table 3**, respectively. The PM6 possesses 3D molecular orientation, as evidenced by obvious (100) diffraction peaks and discernable (010) diffraction peaks in both OOP and IP directions of PM6 films. The OOP (010) and IP (100) diffraction peaks can be synchronously perceived from the profiles of neat PY-IT films, manifesting the preferred face-on orientation of PY-IT. It should be highlighted that the neat F-Pt films display multiple strong and narrow diffraction peaks ranging from 0.60 $Å^{-1}$ to 1.85 $Å^{-1}$ in OOP and IP direction, indicating the long-range ordered and highly crystalline molecular packing of F-Pt. The highly crystalline nature of F-Pt may induce it as crystallinity agent for ameliorating molecular packing of host materials, and similar phenomenon has been reported in the literature.[68, 69] When incorporating 0.2 wt% F-Pt into PY-IT films, the face-on orientation of PY-IT is more ordered for effective electron transport in films, which can be well supported by apparently elevated OOP (010) and IP (100) diffraction intensity of PY-IT:F-Pt films. The OOP (010) and IP (100) diffraction peaks for PM6/PY-IT films are located at 1.623 Å and 0.286 Å, which is close to the position of neat PY-IT and PM6 films, manifesting that the π-π stacking and lamellar stacking in LbL films is largely determined by PY-IT and PM6, respectively. The d-spacing of π-π stacking in LbL films can be gradually decreased along with the incorporation of F-Pt, resulting in tighter molecular stacking of PY-IT for effective electron transport, which can be supported by the gradually redshifted OOP (010) diffraction peak induced by F-Pt. The CCL values of π-π stacking in LbL films can be increased from 61.03 Å to 76.49 Å along with the incorporation of F-Pt, manifesting the higher crystallinity degree of PY-IT caused by F-Pt. Meanwhile, with the incorporation of F-Pt, the characteristic signal at 0.40 Å originated from lamellar stacking of PY-IT is gradually distinguishable in LbL films together with more intense π-π stacking intensity, indicating the formation of more ordered face-on orientation of PY-IT induced by F-Pt. The more ordered face-on orientation and increased crystallinity degree of PY-IT should be conductive to electron transport along the normal direction of substrate, which well accords with the μ_e improvement of LbL films by incorporating F-Pt.

Storage stability of APSCs was investigated for the cells stored in N_2 filled globe box. The evolution plots of normalized PCE and normalized FF with storage time are displayed in **Figure S4**. The optimal LbL APSCs retain more than 85% of the initial PCE after 1296 h storage, only about 81% of initial PCE can be kept for the PM6/PY-IT based APSCs after the same storage time. Meanwhile, the FFs of optimized LbL APSCs can be well kept with over 92% of initial value after 1296 h storage. The storage stability of LbL APSCs can be improved by incorporating appropriate F-Pt as additive in acceptor layer.

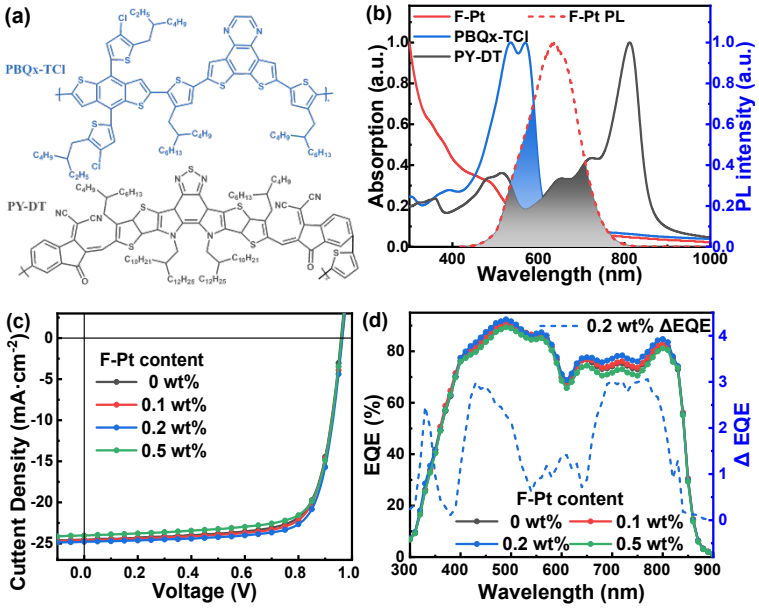

Figure 9. a) Chemical structures of PBQx-TCl and PY-DT. **b)** Absorption spectra of PBQx-TCl, PY-DT, F-Pt films and normalized PL spectrum of F-Pt. **c)** *J*–*V* curves and **d)** EQE spectra of PBQx-TCl/PY-DT based LbL APSCs with or without F-Pt incorporation and ΔEQE between the control cells and the optimized cells.

Table 4. Parameters of PBQx-TCl/PY-DT based LbL APSCs.

F-Pt content [wt%]	J_{SC} [mA·cm^{-2}]	Cal. J_{SC} [mA·cm^{-2}]	V_{OC} [V]	FF [%]	PCE (Ave. ±Dev.) [%]	R_S [Ω·cm^2]	R_{SH} [Ω·cm^2]
0	24.53	23.37	0.96	74.68	17.57 (17.39±0.15)	3.28	887
0.1	24.62	23.65	0.96	75.19	17.84 (17.72±0.10)	2.83	1057
0.2	24.79	23.76	0.96	76.53	18.29 (18.14±0.11)	2.81	1091
0.5	24.04	22.91	0.96	75.41	17.41 (17.21±0.19)	3.05	1049

The efficient donor Poly[9-(5-{4,8-bis[4-chloro-5-(2-ethylhexyl)thiophen-2-yl]-6-methylthieno[2',3':4,5]benzo[b]thiophen-2-yl}-4-(2-butyloctyl)thiophen-2-yl)-6-[4-(2-butyloctyl)-5-methylthiophen-2-yl]dithieno[3,2-f:2',3'-h]quinoxaline] (PBQx-TCl) and acceptor Poly[2-{2-[(E)-[3,9-bis(2-butyloctyl)-12,13-bis(2-decyltetradecyl)-10-{[(2E)-1-(dicyanomethylidene)-5-(5-

methylthiophen-2-yl)-3-oxo-2,3-dihydro-1H-inden-2-ylidene]methyl}-3a,4b,7b,8a,11a,12,13,13b-octahydro[1,2,5]thiadiazolo[4,3-e]thieno[2',3':4,5]thieno[3,2-b]thieno[2'',3'':4',5']thieno[2',3':4,5] pyrrolo[3,2-g]indol-2-yl]methylidene]-5-methyl-3-oxo-2,3-dihydro-1H-indenylidene} propanedinitrile] (PY-DT) were selected to verify the universality of F-Pt incorporation on the PCE improvement. The chemical structures of PBQx-TCl and PY-DT are displayed in **Figure 9a**. The absorption spectra of PBQx-TCl, PY-DT, F-Pt films and normalized PL spectrum of F-Pt films are shown in **Figure 9b**. There are two absorption peaks at 535 nm and 570 nm of PBQx-TCl films, which are less than the PL emission peak at 635 nm of F-Pt films. Although there is some spectral overlapping between the absorption spectrum of PBQx-TCl and PL spectrum of F-Pt, the energy transfer from F-Pt to PBQx-TCl should be insufficient due to the relatively low energy of PL emission of F-Pt. Meanwhile, the energy transfer from F-Pt to PY-DT should be efficient due to the large spectral overlapping and relatively large energy of F-Pt emission in comparison with the energy of PY-DT absorption. The *J-V* curves of the PBQx-TCl/PY-DT based APSCs were measured under simulated AM 1.5 G illumination and are shown in **Figure 9c**. The corresponding parameters of LbL APSCs with or without F-Pt incorporation in PY-DT layer are listed in **Table 4.** After incorporating 0.2 wt% F-Pt, the PCE increases from 17.57% to 18.29% with elevated J_{SC} (from 24.53 mA·cm^{-2} to 24.79 mA·cm^{-2}) and improved FF (from 74.68% to 76.53%). The EQE values of the optimized APSCs are significantly increased in the spectral range from 650 nm ~ 800 nm, as shown in **Figure 9d**. The increased EQE values in this wavelength range should be attributed to the energy transfer from F-Pt to PY-DT and the prolonged exciton lifetime of PY-DT. The relatively low EQE improvement in the spectral range from 500 nm ~ 600 nm can be observed from the ΔEQE spectrum, as shown in **Figure 9d**, which should be attributed to insufficient energy transfer from F-Pt to PBQx-TCl caused by the relatively low emission energy of F-Pt. The spectral overlapping between PL spectrum of F-Pt and absorption spectrum of PBQx-TCl is rather small in the wavelength range of absorption edge of PBQx-TCl. According to the two series of experimental results on PM6/PY-IT or PBQx-TCl/PY-DT, the performance of LbL APSCs can be efficiently enhanced by incorporating triplet material with long lifetime. The exciton diffuse distance can be prolonged through energy transfer process, which should play a vital role in enhancing the exciton dissociation efficiency, especially in this kind of LbL PSCs. This work indicates that Pt complex

incorporation should be an efficient strategy for improving the performance of LbL PSCs.

Conclusions

In summary, series of APSCs were fabricated by employing layer-by-layer deposition method with donors PM6 or PBQx-TCl and the acceptors PY-IT or PY-DT. The triplet materials F-Pt was incorporated into acceptor layer as energy donor additive, which can transfer its energy to donors or acceptors. Such energy transfer can be confirmed from the corresponding PL spectra and TRPL spectra of neat, blend and LbL films. Additionally, it is found that the incorporation of F-Pt into the PY-IT layer can improve the π–π stacking of acceptor molecules and increasing the electron mobility of PY-IT layer. A champion PCE of 17.14% was achieved in LbL APSCs with PM6/PY-IT:F-Pt as active layer benefiting from the enhanced J_{SC} of 24.42 mA·cm^{-2} and FF of 73.87%, which is higher than 15.86% PCE of PM6/PY-IT APSCs. For the PBQx-TCl/PY-DT based LbL APSCs, a high PCE of 18.29% was achieved when 0.2 wt% F-Pt is introduced into PY-DT layer. This work provides an effective way to enhance the performance of LbL APSCs by incorporating Pt complex through improving the exciton utilization efficiency.

Supporting Information

Supporting Information is available from the Wiley Online Library or from the author.

Acknowledgements

This work was supported by the Fundamental Research Funds for the Central Universities (2022JBZY012), National Natural Science Foundation of China (Grant Nos. 62175011, 62105017 and 62205276), Natural Science Foundation of Beijing (4232073, 1232029), National Research Foundation of Korea (2023K2A9A2A06059546). Natural Science Foundation of Hebei Province (F2023105002). W.-Y. Wong thanks for the financial support of the Hong Kong Research Grants Council (PolyU 15307321), RGC Senior Research Fellowship Scheme (SRFS2021-5S01), Research Institute for Smart Energy (CDAQ), and Ms. Clarea Au for the Endowed Professorship in Energy (847S).

Notes and references

1. Ding, G.; Chen, T.; Wang, M.; Xia, X.; He, C.; Zheng, X.; Li, Y.; Zhou, D.; Lu, X.; Zuo, L., Solid additive-assisted layer-by-layer processing for 19% efficiency binary organic solar cells. *Nano-Micro Letters* **2023,** *15* (1), 92.

2. Yi, J.; Zhang, G.; Yu, H.; Yan, H., Advantages, challenges and molecular design of different material types used in organic solar cells. *Nature Reviews Materials* **2024,** *9* (1), 46-62.

3. Shen, Y. F.; Zhang, H.; Zhang, J.; Tian, C.; Shi, Y.; Qiu, D.; Zhang, Z.; Lu, K.; Wei, Z., In situ absorption characterization guided slot‐die‐coated high‐performance large‐area flexible organic solar cells and modules. *Advanced Materials* **2023,** *35* (10), 2209030.

4. Li, D.; Deng, N.; Fu, Y.; Guo, C.; Zhou, B.; Wang, L.; Zhou, J.; Liu, D.; Li, W.; Wang, K., Fibrillization of non‐fullerene acceptors enables 19% efficiency pseudo‐bulk heterojunction organic solar cells. *Advanced Materials* **2023,** *35* (6), 2208211.

5. Liu, S.; Yuan, J.; Deng, W.; Luo, M.; Xie, Y.; Liang, Q.; Zou, Y.; He, Z.; Wu, H.; Cao, Y., High-efficiency organic solar cells with low non-radiative recombination loss and low energetic disorder. *Nature Photonics* **2020,** *14* (5), 300-305.

6. Zhan, L.; Li, S.; Xia, X.; Li, Y.; Lu, X.; Zuo, L.; Shi, M.; Chen, H., Layer‐by‐layer processed ternary organic photovoltaics with efficiency over 18%. *Advanced Materials* **2021,** *33* (12), 2007231.

7. Gui, R.; Xian, K.; Shi, Y.; Zhang, W.; Qiao, J.; Fu, Z.; Wang, J.; Cui, F.; Wang, Q.; Wong, V. K., Unraveling High Reproducibility and Broad Composition Tolerance in High‐Efficiency Organic Solar Cells via Sequential Deposition. *Advanced Energy Materials* **2023,** *13* (44), 2302029.

8. Sun, Y.; Nian, L.; Kan, Y.; Ren, Y.; Chen, Z.; Zhu, L.; Zhang, M.; Yin, H.; Xu, H.; Li, J., Rational control of sequential morphology evolution and vertical distribution toward 17.18% efficiency all-small-molecule organic solar cells. *Joule* **2022,** *6* (12), 2835-2848.

9. Fu, H.; Peng, Z.; Fan, Q.; Lin, F. R.; Qi, F.; Ran, Y.; Wu, Z.; Fan, B.; Jiang, K.; Woo, H. Y., A Top‐Down Strategy to Engineer ActiveLayer Morphology for Highly Efficient and Stable All‐Polymer Solar Cells. *Advanced Materials* **2022,** *34* (33), 2202608.

10. Huang, X.; Cheng, Y.; Fang, Y.; Zhang, L.; Hu, X.; Jeong, S. Y.; Zhang, H.; Woo, H. Y.; Wu, F.; Chen, L., A molecular weight-regulated sequential deposition strategy enabling semitransparent organic solar cells with the light utilization efficiency of over 5%. *Energy & Environmental Science* **2022,** *15* (11), 4776-4788.

11. Kim, W.; Oh, J.; Park, J.; Sun, Z.; Park, J.; Mai, T. L. H.; Kim, S.; Yang, C., Building-up relations between intra-and intermolecular interactions, miscibility, and performance for low-cost, efficient fully non-fused acceptor-based organic solar cells. *Nano Energy* **2023,** *117*, 108853.

12. Jiang, K.; Zhang, J.; Peng, Z.; Lin, F.; Wu, S.; Li, Z.; Chen, Y.; Yan, H.; Ade, H.; Zhu, Z., Pseudo-bilayer architecture enables high-performance organic solar cells with enhanced exciton diffusion length. *Nature Communications* **2021,** *12* (1), 468.

13. Bi, P.; Zhang, S.; Chen, Z.; Xu, Y.; Cui, Y.; Zhang, T.; Ren, J.; Qin, J.; Hong, L.; Hao, X., Reduced non-radiative charge recombination enables organic photovoltaic cell approaching 19% efficiency. *Joule* **2021,** *5* (9), 2408-2419.

14. de Sousa, L. E.; de Paiva, L. S. R.; da Silva Filho, D. A.; Sini, G.; de Oliveira Neto, P. H., Assessing the effects of increasing conjugation length on exciton diffusion: from small molecules to the polymeric limit. *Physical Chemistry Chemical Physics* **2021,** *23* (29), 15635-15644.

15. Sajjad, M. T.; Ruseckas, A.; Samuel, I. D., Enhancing exciton diffusion length provides new opportunities for organic photovoltaics. *Matter* **2020,** *3* (2), 341-354.

16. Li, Y.; Wu, J.; Yi, X.; Liu, Z.; Liu, H.; Fu, Y.; Liu, J.; Xie, Z., Layer-by-layer blade-coated organic solar cells with non-halogenated solvents and non-halogenated additive via adjusting morphology and crystallization. *Journal of Materials Chemistry C* **2023,** *11* (39), 13263-13273.

17. Xu, W.; Zhu, X.; Ma, X.; Zhou, H.; Li, X.; Jeong, S. Y.; Woo, H. Y.; Zhou, Z.; Sun, Q.; Zhang, F., Achieving 15.81% and 15.29% efficiency of all-polymer solar cells based on layer-by-layer and bulk heterojunction structures. *Journal of Materials Chemistry A* **2022,** *10* (25), 13492-13499.

18. Li, Q.; Wang, L.-M.; Liu, S.; Guo, L.; Dong, S.; Ma, G.; Cao, Z.; Zhan, X.; Gu, X.; Zhu, T., Vertical composition distribution and crystallinity regulations enable high-performance polymer solar cells with> 17% efficiency. *ACS Energy Letters* **2020,** *5* (11), 3637-3646.

19. Cui, Y.; Zhang, S.; Liang, N.; Kong, J.; Yang, C.; Yao, H.; Ma, L.; Hou, J., Toward Efficient Polymer Solar Cells Processed by a Solution‐Processed Layer‐By‐Layer Approach. *Advanced Materials* **2018,** *30* (34), 1802499.

20. Ma, X.; Xu, W.; Liu, Z.; Jeong, S. Y.; Xu, C.; Zhang, J.; Woo, H. Y.; Zhou, Z.; Zhang, F., Over 18.1% efficiency of layer-by-layer polymer solar cells by enhancing exciton utilization near the ITO electrode. *ACS Applied Materials & Interfaces* **2023,** *15* (5), 7247-7254.

21. Xu, W.; Zhang, M.; Ma, X.; Zhu, X.; Jeong, S. Y.; Woo, H. Y.; Zhang, J.; Du, W.; Wang, J.; Liu, X., Over 17.4% Efficiency of Layer‐by‐Layer All‐Polymer Solar Cells by Improving Exciton Utilization in Acceptor Layer. *Advanced Functional Materials* **2023,** *33* (28), 2215204.

22. Tian, H.; Xu, W.; Liu, Z.; Xie, Y.; Zhang, W.; Xu, Y.; Jeong, S. Y.; Zhang, F.; Weng, N.; Zhang, Z., Over 18.8% Efficiency of Layer‐By‐Layer Organic Photovoltaics Enabled by Ameliorating Exciton Utilization in Acceptor Layer. *Advanced Functional Materials* **2024**, *34* (16), 2313751.

23. Du, X.; Yuan, Y.; Zhou, L.; Lin, H.; Zheng, C.; Luo, J.; Chen, Z.; Tao, S.; Liao, L. S., Delayed fluorescence emitter enables near 17% efficiency ternary organic solar cells with enhanced storage stability and reduced recombination energy loss. *Advanced Functional Materials* **2020,** *30* (15), 1909837.

24. Park, S. Y.; Chandrabose, S.; Price, M. B.; Ryu, H. S.; Lee, T. H.; Shin, Y. S.; Wu, Z.; Lee, W.; Chen, K.; Dai, S., Photophysical pathways in efficient bilayer organic solar cells: The importance of interlayer energy transfer. *Nano Energy* **2021,** *84*, 105924.

25. Luo, D.; Jiang, Z.; Tan, W. L.; Zhang, L.; Li, L.; Shan, C.; McNeill, C. R.; Sonar, P.; Xu, B.; Kyaw, A. K. K., Non‐Fused Ring Acceptors Achieving over 15.6% Efficiency Organic Solar Cell by Long Exciton Diffusion Length of Alloy‐Like Phase and Vertical Phase Separation Induced by Hole Transport Layer. *Advanced Energy Materials* **2023,** *13* (6), 2203402.

26. Chen, Z.; He, C.; Ran, P.; Chen, X.; Zhang, Y.; Zhang, C.; Lai, R.; Yang, Y. M.; Chen, H.; Zhu, H., Ultrafast energy transfer from polymer donors facilitating spectral uniform photocurrent generation and low energy loss in high-efficiency nonfullerene organic solar cells. *Energy & Environmental Science* **2023,** *16* (8), 3373-3380.

27. Zhang, M.; Ivan, M. N. A. S.; Sun, Y.; Li, Z.; Saha, S.; Ahmed, S.; Liu, H.; Wang, Y.; Tsang, Y. H.; Wong, W.-Y., A platinum-based photothermal polymer with intermolecular/ligand-to-ligand charge transfer for efficient and sustainable solar-powered desalination. *J. Mater. Chem. A* **2024**, *12, 9055–9065*

28. Xu, X.; Feng, K.; Bi, Z.; Ma, W.; Zhang, G.; Peng, Q., Single‐junction polymer solar cells with 16.35% efficiency enabled by a platinum (II) complexation strategy. *Advanced materials* **2019,** *31* (29), 1901872.

29. Yao, E.-P.; Tsai, Y.-J.; Hsu, W.-C., An investigation of organic photovoltaics improvement via extension of the exciton lifetime. *Physical Chemistry Chemical Physics* **2015,** *17* (8), 5826-5831.

30. Yang, L.; Gu, W.; Lv, L.; Chen, Y.; Yang, Y.; Ye, P.; Wu, J.; Hong, L.; Peng, A.; Huang, H., Triplet tellurophene‐based acceptors for organic solar cells. *Angewandte Chemie* **2018,** *130* (4), 1108-1114.

31. Wan, Z.; Yang, J.; Liu, Y.; Wang, S.; Zhong, Y.; Li, C.; Zhang, Z.; Xing, G.; Huettner, S.; Tao, Y., Cyclometalated Pt complex-based random terpolymers for efficient polymer solar cells. *Polymer*

Chemistry **2017,** *8* (32), 4729-4737.

32. Qian, M.; Zhang, R.; Hao, J.; Zhang, W.; Zhang, Q.; Wang, J.; Tao, Y.; Chen, S.; Fang, J.; Huang, W., Dramatic Enhancement of Power Conversion Efficiency in Polymer Solar Cells by Conjugating Very Low Ratio of Triplet Iridium Complexes to PTB7. *Advanced Materials (Deerfield Beach, Fla.)* **2015,** *27* (23), 3546-3552.

33. Kim, H.-T.; Seo, J. H.; Ahn, J. H.; Baek, M.-J.; Um, H.-D.; Lee, S.; Roh, D.-H.; Yum, J.-H.; Shin, T. J.; Seo, K., Customized energy down-shift using iridium complexes for enhanced performance of polymer solar cells. *ACS Energy Letters* **2016,** *1* (5), 991-999.

34. Xue, Z.; Wang, S.; Yang, J.; Zhong, Y.; Qian, M.; Li, C.; Zhang, Z.; Xing, G.; Huettner, S.; Tao, Y., Enhanced power conversion efficiency in iridium complex-based terpolymers for polymer solar cells. *npj Flexible Electronics* **2018,** *2* (1), 1.

35. Yao, Z.; Tao, X.; You, D.; Wang, J.; Lv, K.; Ma, H.; Tao, Y., All-small-molecule organic solar cells based on cyclometalated tris-Ir (III) complexes as donor materials. *Organic Electronics* **2023,** *120*, 106857.

36. Zhang, M.; Ma, X.; Zhang, H.; Zhu, L.; Xu, L.; Zhang, F.; Tsang, C.-S.; Lee, L. Y. S.; Woo, H. Y.; He, Z., Metallated terpolymer donors with strongly absorbing iridium complex enables polymer solar cells with 16.71% efficiency. *Chemical Engineering Journal* **2022,** *430*, 132832.

37. Xu W.; Ma X.; Son J. H.; Jeong S. Y.; Niu L.; Xu C.; Zhang S.; Zhou Z.; Gao J.; Woo H. Y.; Zhang J.; Wang J.; Zhang F., Smart Ternary Strategy in Promoting the Performance of Polymer Solar Cells Based on Bulk-Heterojunction or Layer-By-Layer Structure. *Small* **2022,** *18* (4), 2104215.

38. Yang, X.; Guo, H.; Xu, X.; Sun, Y.; Zhou, G.; Ma, W.; Wu, Z., Enhancing molecular aggregations by intermolecular hydrogen bonds to develop phosphorescent emitters for high‐performance near‐infrared OLEDs. *Advanced Science* **2019,** *6* (7), 1801930.

39. Liu, Z.; Zhang M.; Zhang L.; Jeong S. Y.; Geng S.; Woo, H. Y.; Zhang J.; Zhang F.; Ma, X., Over 19.1% efficiency for sequentially spin-coated polymer solar cells by employing ternary strategy. *Chemical Engineering Journal* **2023,** *471*, 144711.

40. Chen, H.; Zhao, T.; Li, L.; Tan, P.; Lai, H.; Zhu, Y.; Lai, X.; Han, L.; Zheng, N.; Guo, L., 17.6%‐Efficient Quasiplanar Heterojunction Organic Solar Cells from a Chlorinated 3D Network Acceptor. *Advanced Materials* **2021,** *33* (37), 2102778.

41. Jin, Y.; Zhang, Y.; Liu, Y.; Xue, J.; Li, W.; Qiao, J.; Zhang, F., Limitations and Perspectives on Triplet‐Material‐Based Organic Photovoltaic Devices. *Advanced Materials* **2019,** *31* (22), 1900690.

42. Tamai, Y.; Murata, Y.; Natsuda, S. i.; Sakamoto, Y. J. A. E. M., How to Interpret Transient Absorption Data?: An Overview of Case Studies for Application to Organic Solar Cells. **2024,** *14* (7), 2301890.

43. Yang, C.; Jiang, M.; Wang, S.; Zhang, B.; Mao, P.; Woo, H. Y.; Zhang, F.; Wang, J. l.; An, Q., Hot‐Casting Strategy Empowers High‐Boiling Solvent‐Processed Organic Solar Cells with Over 18.5% Efficiency. *Advanced Materials* **2024,** *36* (3), 2305356.

44. Sun, R.; Wu, Y.; Yang, X.; Gao, Y.; Chen, Z.; Li, K.; Qiao, J.; Wang, T.; Guo, J.; Liu, C., Single‐junction organic solar cells with 19.17% efficiency enabled by introducing one asymmetric guest acceptor. *Advanced Materials* **2022,** *34* (26), 2110147.

45. An, Q.; Wang, J.; Gao, W.; Ma, X.; Hu, Z.; Gao, J.; Xu, C.; Hao, M.; Zhang, X.; Yang, C., Alloy-like ternary polymer solar cells with over 17.2% efficiency. *Science Bulletin* **2020,** *65* (7), 538-545.

46. Zhang H.; Liu M.; Zhao X.; Ma X.; Yuan G.; Li J.; Zhang F., Photomultiplication type quasi-planar

all-polymer photodetectors with tunable response range. *Applied Physics Letters* **2023,** *123*, 111101.

47. He, C.; Pan, Y.; Lu, G.; Wu, B.; Xia, X.; Ma, C. Q.; Chen, Z.; Zhu, H.; Lu, X.; Ma, W., Versatile sequential casting processing for highly efficient and stable binary organic photovoltaics. *Advanced Materials* **2022,** *34* (33), 2203379.

48. Brus, V., Light dependent open-circuit voltage of organic bulk heterojunction solar cells in the presence of surface recombination. *Organic Electronics* **2016,** *29*, 1-6.

49. Rahimi Chatri, A.; Torabi, S.; Le Corre, V. M.; Koster, L. J. A., Impact of electrodes on recombination in bulk heterojunction organic solar cells. *ACS applied materials & interfaces* **2018,** *10* (14), 12013-12020.

50. Liao, Q.; Kang, Q.; Yang, Y.; An, C.; Xu, B.; Hou, J., Tailoring and modifying an organic electron acceptor toward the cathode interlayer for highly efficient organic solar cells. *Advanced Materials* **2020,** *32* (7), 1906557.

51. Vartanian, M.; de la Cruz, P.; Biswas, S.; Sharma, G. D.; Langa, F., Panchromatic ternary organic solar cells with 9.44% efficiency incorporating porphyrin-based donors. *Nanoscale* **2018,** *10* (25), 12100-12108.

52. Zhao, Z.; Liu, B.; Xu, C.; Li, L.; Liu, M.; Yang, K.; Jeong, S. Y.; Woo, H. Y.; Yuan, G.; Li, W., Highly stable photomultiplication-type organic photodetectors with single polymers containing intramolecular traps as the active layer. *Journal of Materials Chemistry C* **2022,** *10* (20), 7822-7830.

53. Sun, R.; Deng, D.; Guo, J.; Wu, Q.; Guo, J.; Shi, M.; Shi, K.; Wang, T.; Xue, L.; Wei, Z., Spontaneous open-circuit voltage gain of fully fabricated organic solar cells caused by elimination of interfacial energy disorder. *Energy & Environmental Science* **2019,** *12* (8), 2518-2528.

54. Zhao, Z.; Liu, M.; Yang, K.; Xu, C.; Guan, Y.; Ma, X.; Wang, J.; Zhang, F., Highly sensitive narrowband photomultiplication‐type organic photodetectors prepared by transfer‐printed technology. *Advanced Functional Materials* **2021,** *31* (43), 2106009.

55. Xu, C.; Zhao, Z.; Kan, L.; Tao, S.; Ma, X.; Zhu, X.; Wang, K.; Zhang, J.; Li, J.; Zhang, F., Colorful Semitransparent Organic Photovoltaics with Record Key Parameters by Optimizing Photon Utilization and Fabry‐Pérot Resonator Electrode. *Advanced Optical Materials* **2024,** *12* (10), 2302285.

56. Yang, X.; Sun, R.; Wang, Y.; Chen, M.; Xia, X.; Lu, X.; Lu, G.; Min, J., Ternary All‐Polymer Solar Cells with Efficiency up to 18.14% Employing a Two‐Step Sequential Deposition. *Advanced Materials* **2023,** *35* (7), 2209350.

57. Mao, H.; Zhang, L.; Wen, L.; Huang, L.; Tan, L.; Chen, Y., Nanoimprint Lithography‐Dependent Vertical Composition Gradient in Pseudo‐Planar Heterojunction Organic Solar Cells Combined with Sequential Deposition. *Advanced Functional Materials* **2023,** *33* (1), 2209152.

58. Lin, Y.; Firdaus, Y.; Isikgor, F. H.; Nugraha, M. I.; Yengel, E.; Harrison, G. T.; Hallani, R.; El-Labban, A.; Faber, H.; Ma, C., Self-assembled monolayer enables hole transport layer-free organic solar cells with 18% efficiency and improved operational stability. *ACS Energy Letters* **2020,** *5* (9), 2935-2944.

59. Han, J.; Xu, H.; Paleti, S. H. K.; Wen, Y.; Wang, J.; Wu, Y.; Bao, F.; Yang, C.; Li, X.; Jian, X., Vertical stratification engineering of insulating poly (aryl ether) s enables 18.6% organic solar cells with improved stability. *ACS Energy Letters* **2022,** *7* (9), 2927-2936.

60. Gao, W.; Liu, T.; Sun, R.; Zhang, G.; Xiao, Y.; Ma, R.; Zhong, C.; Lu, X.; Min, J.; Yan, H., Dithieno [3, 2‐b: 2′, 3′‐d] pyrrol‐Fused Asymmetrical Electron Acceptors: A Study into the Effects of Nitrogen‐Functionalization on Reducing Nonradiative Recombination Loss and Dipole Moment on Morphology. *Advanced Science* **2020,** *7* (5), 1902657.

61. Wang, R.; Zhang, D.; Xie, S.; Wang, J.; Zheng, Z.; Wei, D.; Sun, X.; Zhou, H.; Zhang, Y., High efficiency non-fullerene organic solar cells without electron transporting layers enabled by Lewis base anion doping. *Nano Energy* **2018,** *51*, 736-744.

62. Le Corre, V. M.; Chatri, A. R.; Doumon, N. Y.; Koster, L. J. A., Charge Carrier Extraction in Organic Solar Cells Governed by Steady‐State Mobilities. *Advanced Energy Materials* **2017,** *7* (22), 1701138.

63. Zhao, X.; Li, X.; Liu, M.; Zhao, Z.; Yang, K.; Liu, P.; Zhang, H.; Li, J.; Ma, X.; Yao, Q.; Sun, Y.; Zhang, F., Photomultiplication-Type All-Polymer Photodetectors and Their Applications in Photoplethysmography Sensor. *Acta Physico Chimica Sinica* **2024,** *40*, 2311021.

64. Chen, Y.; Ye, P.; Zhu, Z.-G.; Wang, X.; Yang, L.; Xu, X.; Wu, X.; Dong, T.; Zhang, H.; Hou, J., Achieving High-Performance Ternary Organic Solar Cells through Tuning Acceptor Alloy. *Advanced Materials* **2017,** *29* (6), 1603154.

65. Jiang, D.; Sun, J.; Ma, R.; Wong, V. K.; Yuan, J.; Gao, K.; Chen, F.; So, S. K.; Hao, X.; Li, G., Extracting charge carrier mobility in organic solar cells through space-charge-limited current measurements. *Materials Science and Engineering: R: Reports* **2024,** *157*, 100772.

66. Wu, W.; Luo, Y.; Dela Peña, T. A.; Yao, J.; Qammar, M.; Li, M.; Yan, H.; Wu, J.; Ma, R.; Li, G., Defining Solid Additive's Pivotal Role on Morphology Regulation in Organic Solar Cells Produced by Layer‐by‐layer Deposition. *Advanced Energy Materials* **2024**, 2400354.

67. Liu, M.; Yao, Q.; Li, S.; Qin, Y.; Jeong, S. Y.; Ma, Y.; Shen, L.; Ma, X.; Yang, K.; Yuan, G., Interfacial Engineering for Photomultiplication Type Organic Photodetectors with Signal‐Noise‐Ratio Over 89 000. *Advanced Optical Materials* **2024**, *12*, 2303216.

68. Xu, W.; Zhang, M.; Liu, Z.; Tian, H.; Zhang, W.; Sun, S.; Jeong, S. Y.; Zhang, F.; Li, X.; Sun, Q., A nonfullerene acceptor as a solid additive realizing a record efficiency of 17.74% in quasi-layered all-polymer solar cells. *Journal of Materials Chemistry A* **2024,** *12*, 4077-4085.

69. Ge, Z.; Qiao, J.; Li, Y.; Song, J.; Zhang, C.; Fu, Z.; Jee, M. H.; Hao, X.; Woo, H. Y.; Sun, Y., Over 18% Efficiency of All‐Polymer Solar Cells with Long‐Term Stability Enabled by Y6 as a Solid Additive. *Advanced Materials* **2023,** *35* (28), 2301906.